buildings

MDPI

Article

Study on the Frost Resistance of Composite Limestone Powder Concrete against Coupling Effects of Sulfate Freeze–Thaw

Mingming Zhang [1], Henglin Lv [1,2,3,*], Shuchun Zhou [1,3], Yuanzhou Wu [1,3], Xiaowei Zheng [1,3,*] and Qiyao Yan [1]

[1] School of Mechanics and Civil Engineering, China University of Mining and Technology, Xuzhou 221116, China; zmm2020cumt@163.com (M.Z.)
[2] Jiangsu Collaborative Innovation Center of Building Energy-Saving and Construction Technology, Jiangsu Vocational Institute of Architectural Technology, Xuzhou 221116, China
[3] Key Laboratory of Engineering Environmental Impact and Structural Safety, China University of Mining and Technology, Xuzhou 221116, China
* Correspondence: henglinlu@yeah.net (H.L.); xwz217@163.com (X.Z.)

Abstract: Concrete in saline or coastal settings exposed to freezing temperatures is frequently affected by coupling actions of sulfate assault and freeze–thaw degradation, reducing the service life of concrete structures significantly. This study conducted an accelerated freeze–thaw cycle test in pure water and Na_2SO_4 solution with a mass proportion of 5% to examine the coupling impact of sulfate freeze–thaw on the frost resistance of composite limestone powder (CLP) concrete. Combined with SEM and XRD methods, the performance degradation mechanisms of composite limestone powder (CLP) concrete in coupling sulfate freeze–thaw conditions were analyzed with a microscopic point of view. The findings demonstrated that limestone powder has a filling effect but the activity is low. When the content is 10~20%, the chemical response is higher than the physical response. The pozzolanic effect of fly ash and slag can improve the pore structure and improve the compactness of concrete. The "superposition effect" of limestone powder, fly ash, and slag can improve the frost resistance of CLP concrete. The scenario of salt freezing cycles has negative effects that are worse than those of water freezing cycles on the antifreeze performance of CLP concrete, including apparent morphology, mass loss, relative dynamic modulus of elasticity, and compressive strength. Sulfate's activation effect boosts slag's activity effect, which significantly promotes the antifreeze performance of concrete subjected to salt frozen cycles over water frozen cycles. The freeze–thaw damage model of CLP concrete under coupling sulfate freeze–thaw is established through theorem analysis and experiment statistics, laying a theoretical framework for the popularization and use of this concrete.

Keywords: sulfate freeze–thaw; composite limestone powder (CLP) concrete; antifreeze capacity; degradation law; damage model

check for updates

Citation: Zhang, M.; Lv, H.; Zhou, S.; Wu, Y.; Zheng, X.; Yan, Q. Study on the Frost Resistance of Composite Limestone Powder Concrete against Coupling Effects of Sulfate Freeze–Thaw. *Buildings* **2023**, *13*, 2776. https://doi.org/10.3390/buildings13112776

Academic Editors: Flavio Stochino and Binsheng (Ben) Zhang

Received: 5 September 2023
Revised: 23 October 2023
Accepted: 2 November 2023
Published: 3 November 2023

Copyright: © 2023 by the authors. Licensee MDPI, Basel, Switzerland. This article is an open access article distributed under the terms and conditions of the Creative Commons Attribution (CC BY) license (https://creativecommons.org/licenses/by/4.0/).

1. Introduction

In order to save resources and protect the environment, limestone powder, fly ash, slag, and other mineral admixtures can be used to partially or completely replace the cement in traditional concrete [1–4]. This kind of concrete with diversified cementitious materials is called composite limestone powder (CLP) concrete [5]. Frost resistance is an important index of concrete durability, which is very important to evaluate the performance of concrete structures in cold regions [6,7]. In the cold environment of saline or coastal areas, because of its water and soil containing a large amount of sulfate, concrete structures often suffer from sulfate attack and freeze–thaw cycle damage coupling, and the damage is more serious than a single factor [8,9]. It will not only affect the appearance of the structure but also bring a lot of economic losses to the maintenance of the structure. Therefore, it is of great significance and value to study the effect of sulfate freeze–thaw coupling on the frost resistance of CLP concrete.

Studies have shown that limestone powder can play a role in filling, nucleation, chemistry, and dilution in concrete [10–14]. Fly ash and slag have certain pozzolanic effects on concrete [15,16]. Different types of mineral admixtures are mixed into concrete in proportion to realize the effective and reasonable matching of different particle sizes, different shapes, and different activities, so as to achieve the complementary purpose of the morphological effect, activity effect, and microaggregate effect. The resulting superposition effect can significantly improve the mechanical properties and durability of concrete [17,18]. In the sulfate attack test, due to the addition of limestone powder, the content of gypsum in the erosion product is increased, which leads to the expansion and cracking of concrete, the decrease in strength, and the decrease in sulfate attack resistance coefficient [19]. At the same water–binder ratio, the sulfate resistance of concrete decreases with the increase in limestone powder content [20]. When limestone powder is mixed with fly ash and slag, it shows a complementary synergistic effect, which can effectively improve the performance of concrete against sulfate attack [21,22].

In the freeze–thaw cycle test, due to the low activity of limestone powder, the content of hydration products in the unit volume of cement-based materials decreases, resulting in a decrease in the bond strength between aggregates and a decrease in the resistance to ice crystal expansion pressure. This further leads to the loss of concrete quality, and this quality loss is positively correlated with the amount of limestone powder. At the same time, the relative dynamic elastic modulus will also decrease [23–25]. For conventional strength grade concrete, the addition of limestone powder has little effect on its frost resistance, but it will lead to the reduction in cementitious materials and the loss of strength, thus affecting the durability of concrete. In order to make up for this problem, it can be compensated by reducing the water–binder ratio of limestone powder concrete [26]. As for low strength concrete, increasing the content of limestone powder from 0% to 20% can improve the resistance to chloride ion penetration but will reduce the frost resistance [27]. The results show that when the content of limestone powder is 5%, the mass loss rate is the smallest and the frost resistance is the highest. When the content of limestone powder is between 5% and 10%, the mass loss rate is lower than that of ordinary concrete and the frost resistance is higher than that of ordinary concrete. However, when the content of limestone powder increases to 15~20%, the mass loss rate of concrete exceeds that of ordinary concrete, and the performance will also be affected [28].

The above studies have confirmed that single or double doping of limestone powder, fly ash, slag, and other mineral admixtures in concrete can change the sulfate resistance and frost resistance of concrete. However, there are few studies on the variation of the frost resistance of CLP concrete mixed with limestone powder, fly ash, and slag under sulfate freeze–thaw coupling, and the interaction mechanism between compounds needs to be further clarified. Therefore, in this paper, the freeze–thaw cycle tests of CLP concrete with different blending ratios were carried out in pure water and Na_2SO_4 solution with mass fraction of 5%, respectively, to study the apparent morphology, mass loss, relative dynamic elastic modulus, and compressive strength of concrete. At the same time, the degradation mechanism of frost resistance of concrete is analyzed from the microscopic point of view. The freeze–thaw damage model of CLP concrete under sulfate freeze–thaw coupling is established, which provides a theoretical reference for the popularization and application of the concrete.

2. Materials and Methods

2.1. Materials

The test materials are as follows:

(1) Cementitious material: P.O 42.5 ordinary Portland cement, with specific surface area of 341 m^2/kg; limestone powder, with specific surface area of 450 m^2/kg; F I grade coal fly ash, with specific surface area of 364 m^2/kg; S95 slag, with specific surface area of 435 m^2/kg.

(2) Aggregate: coarse aggregate is continuous graded crushed stone with particle size of 5~31.5 mm; the natural river sand is selected as the fine aggregate, with the fineness modulus of 2.69 and the apparent density of 2690 kg/m^3.
(3) Mixing water: commonly used tap water.
(4) Water reducer: PCA-I polycarboxylate high-performance water reducer with a value of 28% of water reduction rate [5].

The mix ratio of CLP concrete is designed with reference to the corresponding national standard and the literature [29–31]. The detailed mix designs are shown in Table 1.

Table 1. Mix ratios of CLP concrete.

Number	Water–Binder Ratio	Material Consumption Per Unit Volume (kg/m^3)								f_{cu} (MPa)
		Cement	Ground Limestone	Fly Ash	Slag	Sand	Stone	Water	Additives	
$L_0F_0S_0$	0.49	345	0	0	0	765	1110	170	4.49	46.3
$L_{10}F_0S_0$	0.49	310	35	0	0	765	1110	170	4.49	41.8
$L_{20}F_0S_0$	0.49	276	69	0	0	765	1110	170	4.49	35.3
$L_{20}F_{30}S_0$	0.49	173	69	103.6	0	765	1110	170	4.49	23.7
$L_{20}F_0S_{30}$	0.49	173	69	0	103.6	765	1110	170	4.49	35.6
$L_{20}F_{15}S_{15}$	0.49	173	69	51.8	51.8	765	1110	170	4.49	32.3

Note: In the table number, L refers to limestone powder, F refers to fly ash, S refers to slag, and the lower right is the replacement ratio. For example, "20" refers to the replacement of 20% cement with equal mass.

2.2. Methods

In this study, the rapid freeze–thaw cycle tests on CLP concrete were carried out in pure water and 5% Na_2SO_4 solution, respectively. The specific test scheme is shown in Table 2. According to the experimental scheme in Table 2, 12 groups of prism specimens with dimensions of 100 mm × 100 mm × 400 mm and 54 groups of cube specimens with dimensions of 100 mm × 100 mm × 100 mm were made. Each group has 3 samples which are used to test the apparent morphology, mass loss, relative dynamic elastic modulus, and compressive strength of CLP concrete after freeze–thaw cycle tests.

Table 2. Experimental scheme of sulfate freeze–thaw resistance of CLP concrete.

Research Content	Number	Limestone Powder Mixing Amount (%)	Fly Ash Mixing Amount (%)	Slag Mixing Amount (%)	Number of Freeze–Thaw Cycles (Times)	Testing Numbers (Groups)
Relative dynamic elastic modulus and mass loss	A-DZ-HX	0	0	0	25, 50, 75, 100	1
	B-DZ-HX	10	0	0		1
	C-DZ-HX	20	0	0		1
	D-DZ-HX	20	30	0		1
	E-DZ-HX	20	0	30		1
	F-DZ-HX	20	15	15		1
	A-DZ-YX	0	0	0		1
	B-DZ-YX	10	0	0		1
	C-DZ-YX	20	0	0		1
	D-DZ-YX	20	30	0		1
	E-DZ-YX	20	0	30		1
	F-DZ-YX	20	15	15		1

Table 2. *Cont.*

Research Content	Number	Limestone Powder Mixing Amount (%)	Fly Ash Mixing Amount (%)	Slag Mixing Amount (%)	Number of Freeze–Thaw Cycles (Times)	Testing Numbers (Groups)
Compressive strength	A-KY-HX	0	0	0	25, 50, 75, 100	5
	B-KY-HX	10	0	0		5
	C-KY-HX	20	0	0		5
	D-KY-HX	20	30	0		5
	E-KY-HX	20	0	30		5
	F-KY-HX	20	15	15		5
	A-KY-YX	0	0	0		4
	B-KY-YX	10	0	0		4
	C-KY-YX	20	0	0		4
	D-KY-YX	20	30	0		4
	E-KY-YX	20	0	30		4
	F-KY-YX	20	15	15		4

Note: The numbering rules in the table are as follows: A, B, C, D, E, F represent $L_0F_0S_0$, $L_1F_0S_0$, $L_2F_0S_0$, $L_2F_3S_0$, $L_2F_0S_3$, $L_2F_{1.5}S_{1.5}$. DZ represents two terms, relative dynamic elastic modulus and mass loss, and KY represents compressive strength. H represents the freeze–thaw cycle in pure water (referred to as "water freeze cycle"). Y represents the freeze–thaw cycle in 5% Na_2SO_4 solution (referred to as "salt freeze cycle"). X represents that the numbers of freeze–thaw cycles were 25, 50, 75, and 100.

The frost resistance tests on CLP concrete were carried out with reference to the relevant literature [32–34]. First of all, the prepared concrete specimens were put into the standard curing room for 24 days and then removed for appearance inspection. Then, the specimens were immersed in water with a temperature of 20 ± 2 °C and 5% Na_2SO_4 solution for 4 days. The liquid was 20 mm higher than the top surface of the specimen during immersion. Finally, the corresponding water freezing cycle and salt freezing cycle tests were carried out on the specimens after 4 days of immersion. The quick freezing test equipment is shown in Figure 1.



Figure 1. Fast freezing test equipment.

The compressive strength of concrete was tested by the YAW-3000 microcomputer controlled electrohydraulic servo pressure testing machine. During the test, continuous uniform loading was applied. Before loading, we ensured that the specimen was located in the middle of the upper and lower bearing plates, and the surface contact between the specimen and the bearing plate was balanced [35,36]. The concrete cube compressive strength test is shown in Figure 2.



Figure 2. Compressive testing on the concrete cube.

3. Results and Discussion

3.1. Apparent Morphology

For the convenience of comparative analysis, Figure 3 divides the apparent morphology of the specimens into left and right columns at the beginning and end of the water freezing cycle. The number of the corresponding concrete formula is marked on the top left or top right of the apparent morphology picture of each specimen. The number of comments can be referred to Table 1. It can be seen from Figure 3 that when the water freezing cycle is 0 times, there are no other defects on the surface of the specimen, except for a small number of tiny pores. After 100 water freezing cycles, the specimen has a darker apparent color due to water absorption and humidity. The apparent morphologies of A-DZ-H100 and B-DZ-H100 specimens did not change significantly. There are a few mortar drops on the surfaces of C-DZ-H100, D-DZ-H100, E-DZ-H100, and F-DZ-F100 specimens, revealing "starry spots" of coarse aggregate. This is similar to the phenomenon observed in references [37,38]. It shows that the damage to the concrete is small within 100 water freezing cycles. In this study, in order to consider the salt freezing cycle and to perform a comparative analysis, only effective data within 100 water freezing cycles were selected.

Figure 4 shows the apparent morphologies of the specimens at the beginning and the end of the salt freezing cycles. It can be found from Figure 4 that the salt freezing cycle has a great influence on the damage and failure of the apparent morphologies of the specimens, and the failure phenomena are similar to those observed in the literature [39]. Among them, some specimens (C-DZ-Y50; D-DZ-Y50 and B-DZ-Y75) were subjected to 50 and 75 salt freezing cycles, respectively. The surface mortar peeled off severely, the coarse aggregate was exposed, and the test was stopped. After 100 salt freezing cycles, the coarse aggregate of the A-DZ-Y100 specimen fell off in a large range, and the apparent morphologies of the specimens became incomplete. The coarse aggregates of E-DZ-Y100 and F-DZ-Y100 specimens were more exposed, and the coarse aggregates of F-DZ-Y100 specimen were more obvious.

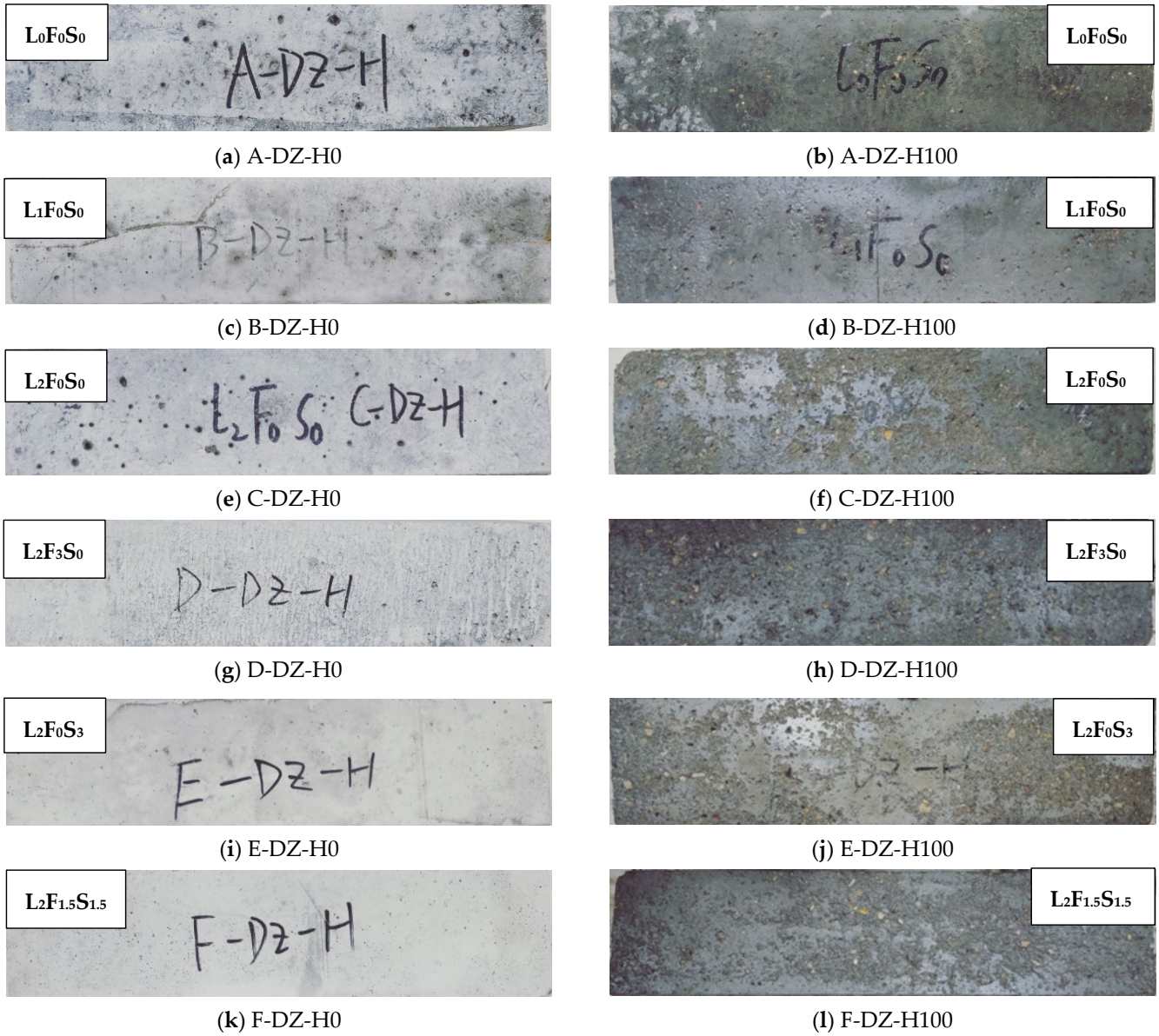
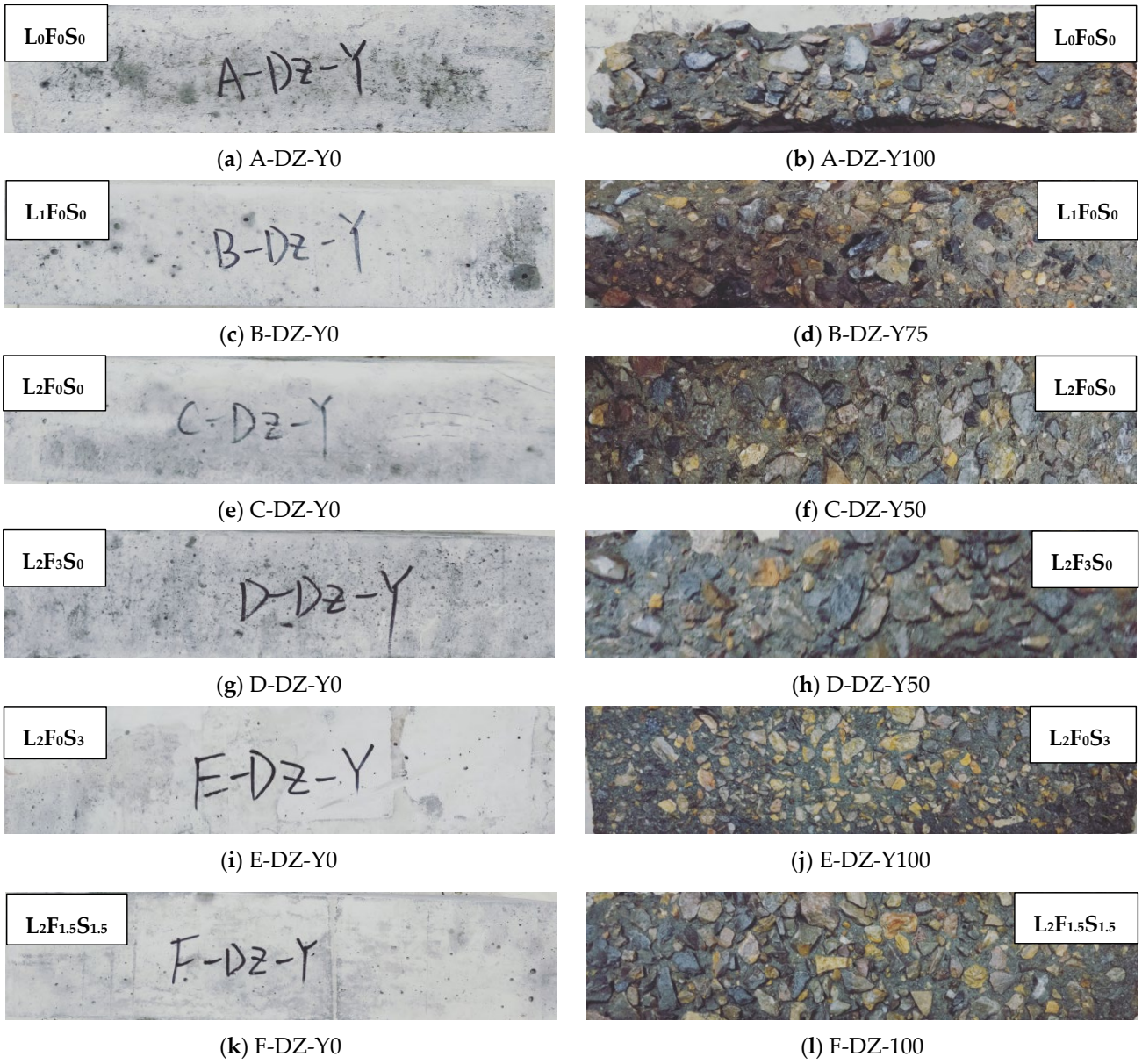


Figure 3. Apparent morphologies of the specimens at the beginning and end of the water freezingcycles.

Comparing the apparent morphologies of the specimens after water freezing cycles and salt freezing cycles, it can be found that the damage of the concrete specimens under salt freezing cycles is much greater than that under water freezing cycles. The reason for this phenomenon is that on the one hand, freeze–thaw damage causes microcracks in concrete, accelerates the invasion of salt solution, and causes expansion damage to concrete; on the other hand, the sulfate solution increases the initial saturation of the pore fluid inside the concrete, which increases the pore wall pressure of the concrete during the freeze–thaw process, thereby aggravating the freeze–thaw damage of the concrete [39,40].



(**a**) A-DZ-Y0 (**b**) A-DZ-Y100

(**c**) B-DZ-Y0 (**d**) B-DZ-Y75

(**e**) C-DZ-Y0 (**f**) C-DZ-Y50

(**g**) D-DZ-Y0 (**h**) D-DZ-Y50

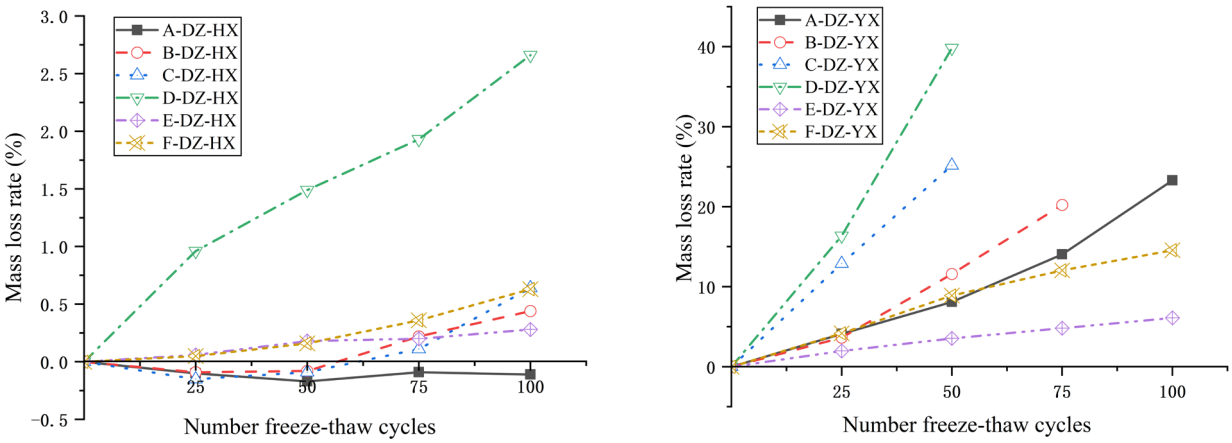
(**i**) E-DZ-Y0 (**j**) E-DZ-Y100

(**k**) F-DZ-Y0 (**l**) F-DZ-100

Figure 4. Apparent morphologies of the specimens at the beginning and end of the salt freezing cycles.

3.2. Mass Loss

Figure 5 shows the mass losses of concrete specimens under different freeze–thaw cycles. It can be found from Figure 5a that the mass loss rate of the specimens did not exceed 3% after 100 water freezing cycles, which was lower than the limit of 5% in the corresponding national standard [32]. This shows that the incorporation of limestone powder, fly ash, and slag has little effect on the mass loss rate of concrete after 100 freeze–thaw cycles. Among them, the mass losses of specimens A, B, and C decrease first and then increase during the water freezing cycles. This is because the quality of the water absorbed by the concrete is greater than the quality of the peeling mortar on its surface, which leads to an increase in the early quality of the specimen during the freeze–thaw cycle [15,37].



(**a**) In pure water (**b**) In 5% Na_2SO_4 solution

Figure 5. Mass losses of the concrete specimens under different freeze–thaw cycles.

It can be found from Figure 5b that the effect of salt freezing cycles on the mass loss of CLP concrete specimens is much greater than that of water freezing cycles. During the salt freezing cycles, the mass loss of the specimen increased. Among them, the mass loss rate of E specimen was the smallest, which was 6.11%. The mass loss rates of B, C, and D specimens reached 20.23%, 25.16%, and 39.83%, respectively, when the salt freezing cycles were 50 and 75. The mass loss was large and the test was stopped. This shows that the coupling effect of sulfate attack and freeze–thaw damage has a great influence on the damage of concrete [5,39].

3.3. Relative Dynamic Modulus of Elasticity

Figure 6 shows the relative dynamic elastic moduli of concrete specimens under different freeze–thaw cycles. It can be seen from Figure 6a that the relative dynamic elastic modulus of the CLP concrete specimen decreases rapidly during the water freeze–thaw cycles. After 100 water freezing cycles, the relative dynamic elastic moduli of the specimens are in the following order: E-DZ-H100 > F-DZ-H100 > A-DZ-H100 > B-DZ-H100 > D-DZ-H100 > C-DZ-H100. Comparing Figure 6b, it can be found that the damage effect of salt freezing cycles on the relative dynamic elastic modulus of concrete is much greater than that of water freezing cycles, but the incorporation of 15% and 30% slag in CLP concrete can effectively improve this performance. After 50 salt freezing cycles, the relative dynamic elastic moduli of C and D specimens decreased to 35.06% and 37.44% of the original values. Below the limit of 60% of the corresponding national standard [32], the test was stopped.

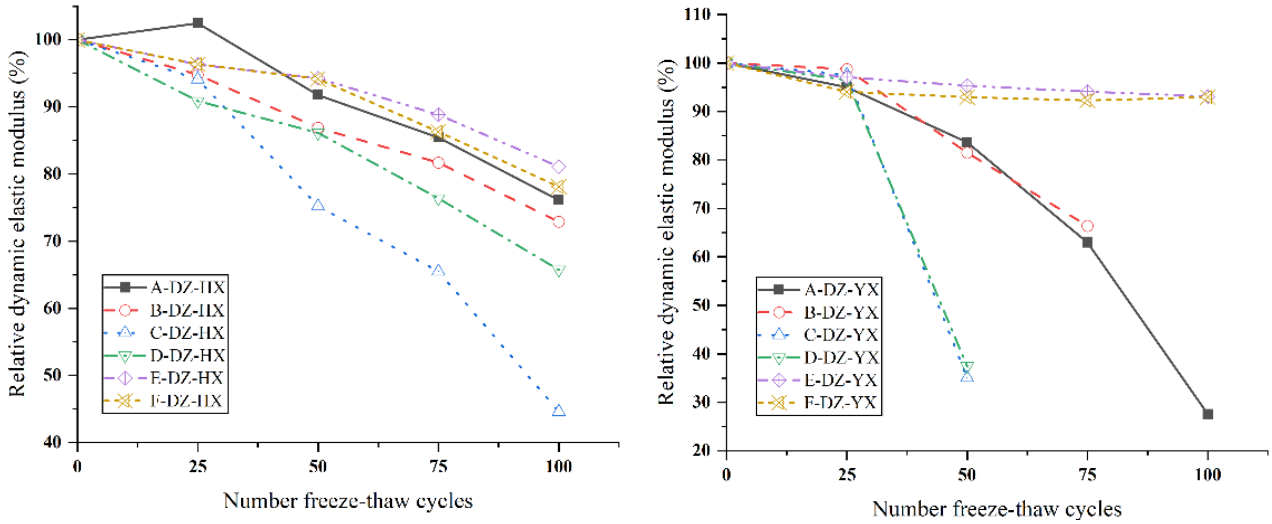
The reasons for the above phenomenon are given as follows.

(1) The relative dynamic elastic modulus of concrete specimens is related to the density of its internal structure [15,37]. Limestone powder has a certain filling effect at the physical level, which can optimize the particle gradation of the cementitious material system. However, its activity effect at the chemical level is low, which will reduce the relative content of hydration products in unit volume concrete, resulting in a decrease in the compactness of concrete and a decrease in the relative dynamic elastic modulus [41,42]. The chemical response of limestone powder with 10~20% content in concrete is higher than its physical response, and the frost resistance of concrete decreases with the increase in the limestone powder content.

(2) The pozzolanic effects of fly ash and slag increase the secondary hydration products, optimize the pore structure, and improve the compactness of concrete [43–45]. However, in the case of the fixed total content of 50%, fly ash is used to replace slag in equal proportion. At the physical level, the specific surface area of fly ash (364 m^2/kg) is less than that of slag (435 m^2/kg), and its particle filling effect in the cementitious system is lower than that of slag, which will make the internal structure of CLP concrete loose

and reduce the compactness. At the chemical level, the activity of fly ash is lower than that of slag, thereby reducing the hydration products in CLP concrete and increasing the porosity.

(3) Sulfate has a certain stimulating effect on the hydration activity of slag in Portland cement [46,47]. As a result, the incorporation of slag in concrete can effectively improve the relative dynamic elastic modulus of the specimens under freeze–thaw cycles, and the improvement effect under the salt freezing cycles is better than that under the water freezing cycles.



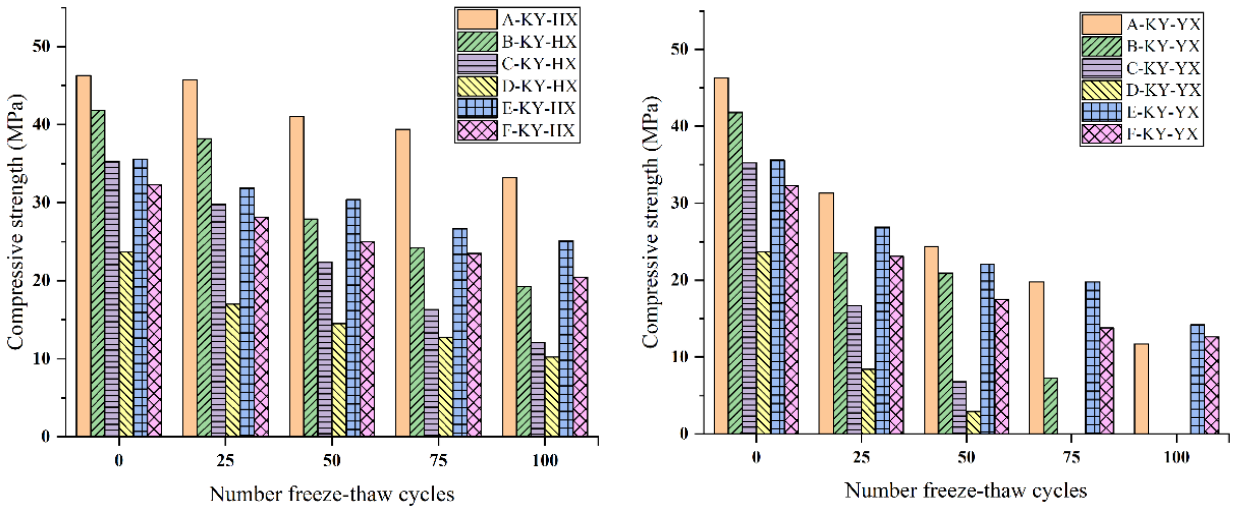
(**a**) In pure water (**b**) In 5% Na_2SO_4 solution

Figure 6. Relative dynamic elastic moduli of the concrete samples under different freeze–thaw cycles.

Therefore, the "superposition effect" of limestone powder, fly ash, and slag can optimize the frost resistance of CLP concrete. Therefore, the frost resistances of the CLP concrete follow the indicated order: $L_{20}F_0S_{30}$ > $L_{20}F_{15}S_{15}$ > $L_0F_0S_0$ > $L_{10}F_0S_0$ > $L_{20}F_{30}S_0$ > $L_{20}F_0S_0$, which corresponds to the relative dynamic elastic modulus.

3.4. Compressive Strength

Figure 7 shows the compressive strengths of the concrete specimens under different freeze–thaw cycles. The letters "A, B, C, D, E, and F" in the specimen number in the figure represent the six concrete formulations of "$L_0F_0S_0$, $L_{10}F_0S_0$, $L_{20}F_0S_0$, $L_{20}F_{30}S_0$, $L_{20}F_0S_{30}$, and $L_{20}F_{15}S_{15}$", respectively. It can be seen from Figure 7 that when the contents of limestone powder are between 10~20%, the compressive strength of concrete will be reduced, and with the increase in the content, the strength loss will be greater. The incorporation of fly ash will reduce the early strength of CLP concrete. The incorporation of slag can improve the compressive strength of CLP concrete. In the freeze–thaw cycles (water freezing or salt freezing), the compressive strengths of all specimens decrease with the increase in the number of freeze–thaw cycles. The damage degree of salt freezing cycles to the compressive strength of the specimen is greater than that of water freezing cycles. The incorporation of limestone powder and fly ash accelerates the loss of compressive strength of concrete specimens in freeze–thaw cycles, but the incorporation of slag can slow down the loss of compressive strength of CLP concrete in freeze–thaw cycles and enhance its frost resistance [45,46].



(**a**) In pure water (**b**) In 5% Na_2SO_4 solution

Figure 7. Compressive strengths of the concrete specimens during different freeze–thaw cycles.

The reason for this phenomenon is that the chemical response of limestone powder with the 10~20% content is higher than the physical response. The compressive strength of concrete decreases with the increase in limestone powder content. When the mineral admixture is fixed at 50%, because the fineness of fly ash is less than that of slag, replacing slag with fly ash in equal proportion will make the internal structure of CLP concrete loose and reduce the strength of the concrete. At the same time, the activity of fly ash is lower than that of slag, which reduces the hydration products in CLP concrete, increases the porosity, and reduces the compressive strength of concrete. In the freeze–thaw cycles, freeze–thaw damage and sulfate freeze–thaw coupling damage will cause damage inside the concrete and reduce its compressive strength, and the latter has a greater impact. At the same time, due to the "superposition effect" of limestone powder, fly ash, and slag, the change law for the compressive strength loss of CLP concrete is the same as that for the relative dynamic elastic modulus.

4. Micro-Degradation Mechanism Analysis

4.1. Analysis of SEM

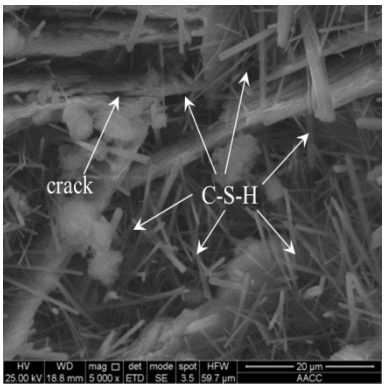
Considering the cost of the tests, this study only focuses on the microstructure and phase composition of the CLP concrete samples after 0, 50, and 100 salt freezing cycles. The SEM images and XRD images are shown in Figures 8 and 9, respectively.

Due to the failure of B specimen sampling during the test, the data were not collected successfully, which was not shown in Figure 8. It can be seen from Figure 8 that the fibrous hydration C-S-H products were found in A, D, and F specimens without salt freezing cycles, and there were more in the A specimen. The spherical particles of fly ash can be clearly seen in the D specimen, indicating that a large amount of fly ash is still not involved in the secondary hydration, and the pozzolanic effect is not fully reflected [43,44]. There are obvious cracks in the cement stone found in specimens A and E, indicating that the concrete specimens have initial defects. The white needle in the C specimen is $CaCO_3$, indicating that the limestone powder mainly plays a filling role, and the activity effect is relatively low [41,48].

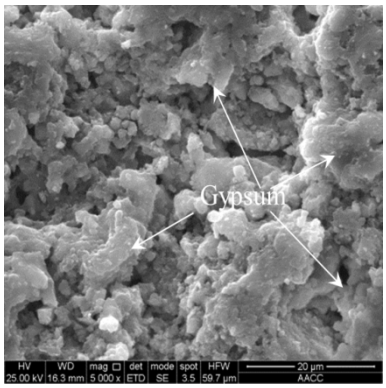
After 50 salt freezing cycles, flocculent fibrous hydration C-S-H products were found in the C specimen, and the microcrystalline nucleation effect of limestone powder was obvious [41,48]. The spherical particles of fly ash can still be clearly seen in the D specimen, and white needle-like and rod-like ettringite were found in E and F specimens, indicating that sulfate had an obvious excitation effect on the hydration activity of slag in Portland cement. The expansion of ettringite produced by hydration fills the internal pores of the

concrete, which can enhance the frost resistance of concrete [39,46]. Flake or block gypsum was found in specimens A, D, and F. Gypsum caused concrete to expand and crack, which reduced its strength and durability. After 50 salt freezing cycles, the damage of specimens C and D was serious, and the test was stopped.

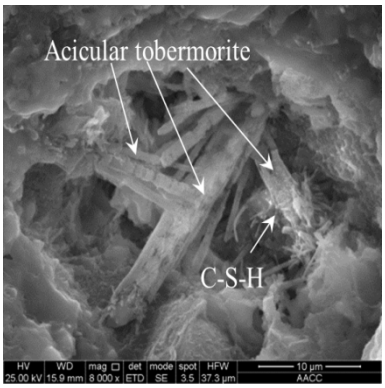
After 100 salt freezing cycles, needle-like thaumasite was found in specimen A, which was shorter and thicker than ettringite crystals. The internal flocculent fibrous hydration C-S-H product was reduced, resulting in low strength and weakened frost resistance. E and F specimens contained many small flocculent fibrous hydration C-S-H products, which have a certain strength and improved frost resistance. There were many flakes or block gypsum in the F specimen, leading to decreases in strength and frost resistance, which were lower than those of the E specimen but higher than those of the A specimen [39].



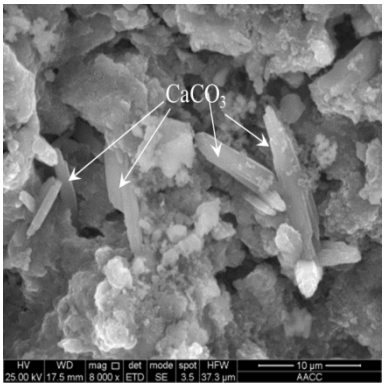
(**a**) A-KY-Y0



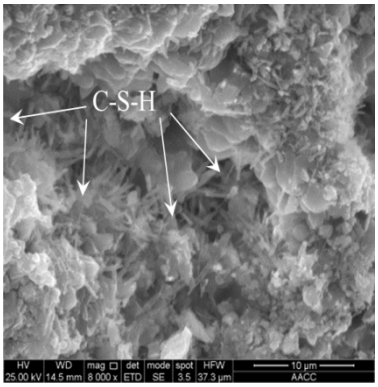
(**b**) A-KY-Y50



(**c**) A-KY-Y100



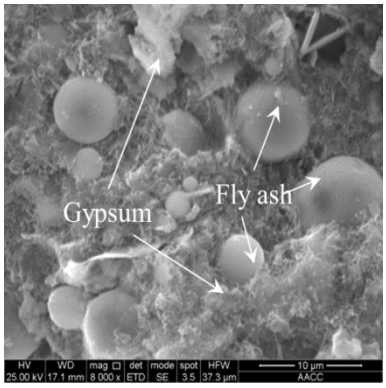
(**d**) C-KY-Y0



(**e**) C-KY-Y50

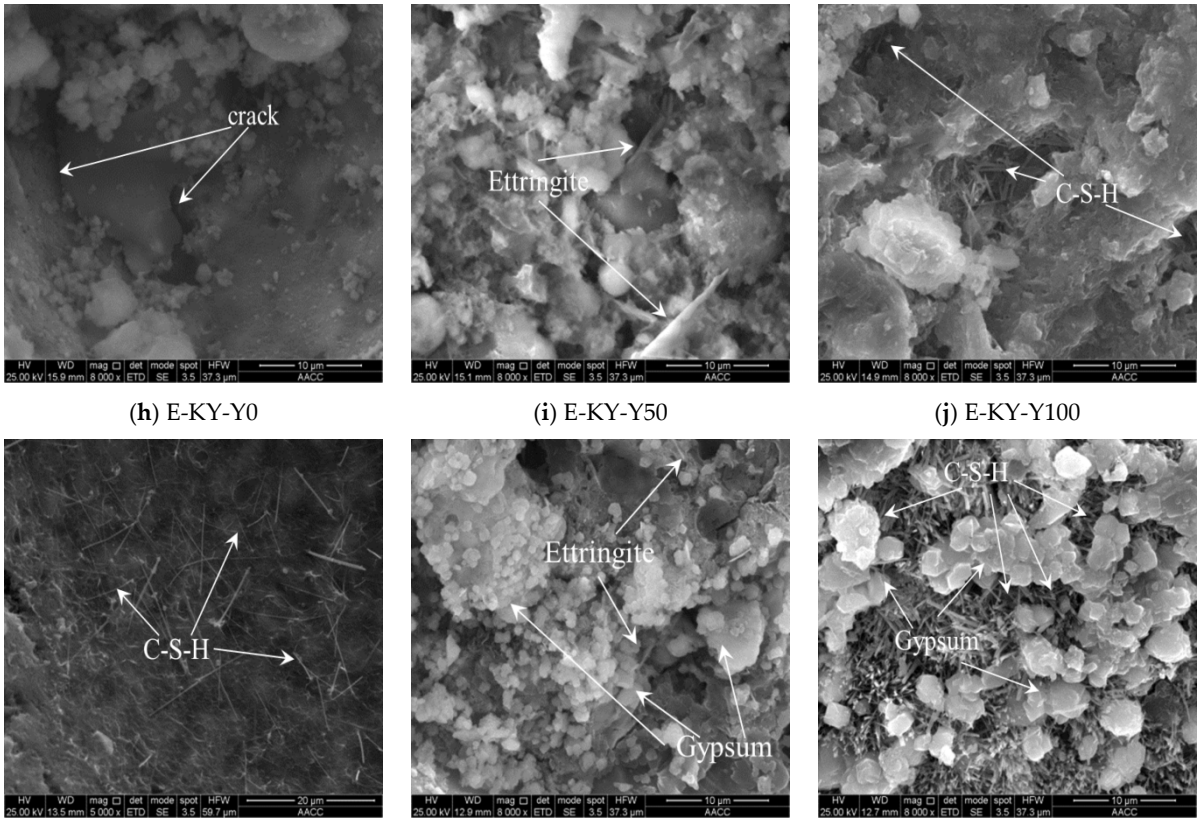


(**f**) D-KY-Y0



(**g**) D-KY-Y50

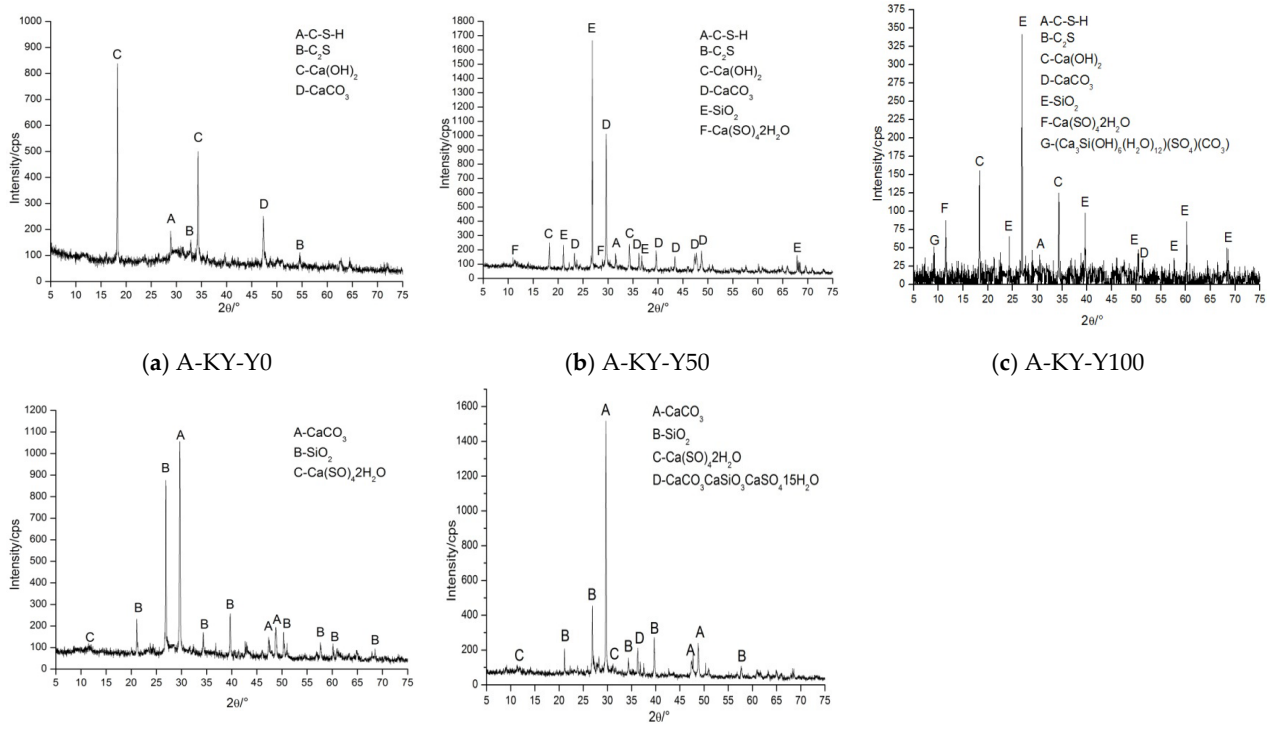
Figure 8. *Cont.*



(**h**) E-KY-Y0 (**i**) E-KY-Y50 (**j**) E-KY-Y100

(**k**) F-KY-Y0 (**l**) F-KY-Y50 (**m**) F-KY-Y100

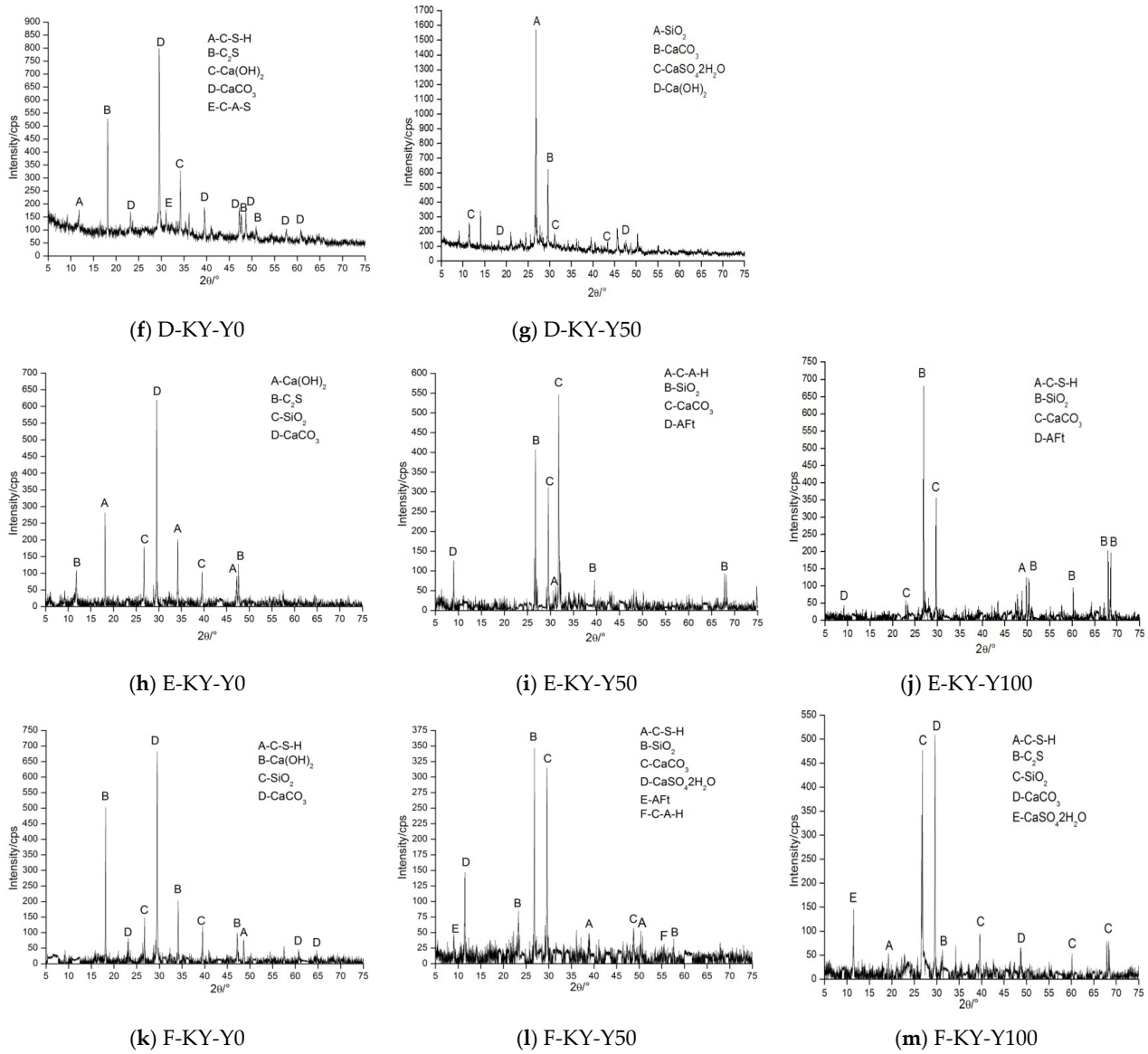
Figure 8. SEM images of the concrete samples after 0, 50, and 100 salt freezing cycles.



(**a**) A-KY-Y0 (**b**) A-KY-Y50 (**c**) A-KY-Y100

(**d**) C-KY-Y0 (**e**) C-KY-Y50

Figure 9. *Cont.*



(**f**) D-KY-Y0 (**g**) D-KY-Y50

(**h**) E-KY-Y0 (**i**) E-KY-Y50 (**j**) E-KY-Y100

(**k**) F-KY-Y0 (**l**) F-KY-Y50 (**m**) F-KY-Y100

Figure 9. XRD images of the concrete samples after 0, 50, and 100 salt freezing cycles.

In summary, it can be seen that ordinary concrete produces gypsum and thaumasite successively in salt freezing cycles. Single limestone powder easily makes the concrete produce thaumasite earlier in the process of salt freezing cycles, and the content is higher. The incorporation of fly ash makes CLP concrete produce gypsum during salt freezing cycles. The incorporation of slag makes CLP concrete produce ettringite in the process of salt freezing cycles, and C-S-H can still be found in the later stage of salt freezing cycles.

4.2. Analysis of XRD

Due to the failure of sampling of specimen B in the test, the data were not collected successfully, which are not shown in Figure 9. It can be seen from Figure 9 that after 50 salt freezing cycles, for the C specimen, when 2θ = 29.672°, the peak value of $CaCO_3$ is the largest. This is mainly affected by the incompletely removed sand and gravel in the sample. When 2θ = 30.792° and 36.277°, gypsum and thaumasite appear. For the D specimen, when 2θ = 26.766°, SiO_2 appears, and the peak value is larger. When 2θ =11.305°, 31.142°, and 43.317°, gypsum appears and exists in many places. When 2θ = 18.17° and 47.226°, $Ca(OH)_2$ appears. When 2θ = 29.528°, there is $CaCO_3$, and the peak value is higher. Due to the influence of incompletely removed sand in the sample, the diffraction peak of SiO_2 is

higher. After 50 salt freezing cycles, the damage of specimens C and D was serious, and the test was stopped.

After 100 salt freezing cycles, for specimen A, when 2θ = 26.852°, the diffraction peak is SiO_2 and exists in many places. When 2θ = 9.126°, thaumasite appears, and the microstructure is shown in Figure 8c. For the E specimen, when 2θ = 49.754°, C-S-H appears. When 2θ = 50.338° and 60.179°, the diffraction peak of SiO_2 appears and exists in many places. For the F specimen, when 2θ = 26.708° and 29.508°, the diffraction peaks of SiO_2 and $CaCO_3$ increase. This is mainly affected by the incompletely removed sand and gravel in the sample. When 2θ = 19.259° and 31.259°, C-S-H and C_2S appear. This shows that the C_2S reaction is slow during the hydration process, and it still exists when the salt freezing cycles are 100.

By analyzing the changes in the composition of each sample during the salt freezing cycles, it can be known that A, D, and F specimens produced gypsum during salt freezing cycles, and thaumasite was found in the A specimen when the salt freezing cycles were 100, resulting in a large decrease in macroscopic strength. The D specimen has low cement content, less cementitious material, low early strength, and slow secondary hydration rate of fly ash, resulting in gypsum mold damage [43,44]. E and F specimens produce ettringite, and early ettringite expands and fills the internal pores of concrete [39,46]. After 100 salt freezing cycles, there is still flocculent fibrous hydration C-S-H product which improves the macroscopic strength of concrete.

4.3. Analysis of MIP

The frost resistance of concrete is closely related to its pore structure [15,39]. In this study, due to the consideration of the cost of the test, only the samples of each concrete formula at the age of 28 d were selected for the MIP test. The pore structure data obtained are used as a supplement to the overall analysis. The pore characteristic parameters of each sample are shown in Table 3.

Table 3. Pore characteristic parameters of individual samples (28 d).

Number	Porosity (%)	Total Pore Volume (mL/g)	Total Pore Area (m^2/g)	Most Probable Pore Size (nm)	Critical Pore Size (nm)	Average Pore Size (nm)	Medium Pore Diameter (nm)
$L_0F_0S_0$	16.53	0.0682	5.947	121.83	182.03	55.7	112.4
$L_{10}F_0S_0$	20.47	0.0981	9.897	100.23	170.32	40.3	72.1
$L_{20}F_0S_0$	22.13	0.1351	7.526	115.43	179.67	49.4	90.2
$L_{20}F_{30}S_0$	21.53	0.1022	8.753	107.21	177.93	44.5	84.3
$L_{20}F_0S_{30}$	18.69	0.0940	11.936	78.34	120.79	31.6	57.1
$L_{20}F_{15}S_{15}$	19.33	0.0965	10.082	95.53	150.97	36.9	64.3

The following can be seen from Table 3. (1) The porosity of concrete with mineral admixtures is higher than that of ordinary concrete ($L_0F_0S_0$), but the most probable pore sizes are smaller than those of ordinary concrete. Among them, the most probable aperture of $L_{20}F_0S_{30}$ concrete is the smallest. (2) For $L_{20}F_0S_{30}$ concrete, its total pore area is the largest, but its total pore volume is not the largest. This is because the pore is assumed to be cylindrical in the mercury injection test. The total pore size is small and the total pore area is large, which means that the pore size is smaller. The average pore size of $L_{20}F_0S_{30}$ concrete is the smallest, which conforms to the law.

By analyzing the pore situation of concrete, it can be found that although the addition of mineral admixtures increases the porosity of concrete to a certain extent, its most probable pore size, critical pore size, average pore size, and median pore size all decrease. However, the freeze–thaw resistance of concrete increases with the decrease in the most probable pore size, critical pore size, and average pore size of the internal pore structure. The concrete with a reasonable pore size distribution has better freeze–thaw resistance [49]. The pore situation of CLP concrete at the age of 28 d in Table 3 can reflect its later freeze–thaw resistance.

4.4. Analysis of Mechanism

Under the coupling effect of sulfate and freeze–thaw, the first freeze–thaw damage of CLP concrete will cause cracks and microcracks in concrete, accelerate the invasion of salt solution, and cause expansion damage to concrete. Secondly, the sulfate solution will increase the initial saturation of the pore fluid inside the concrete, resulting in an increase in the pore wall pressure of the concrete during the freeze–thaw process. At the same time, the pressure generated by the supersaturated crystallization of the sulfate solution in the pores will also aggravate the freeze–thaw damage. The coupling effect of sulfate attack and freeze–thaw cycles makes the damage degree of CLP concrete in the process of salt freeze–thaw cycles much larger than that of water freeze–thaw cycles. However, sulfate has a certain stimulating effect on the hydration activity of slag in Portland cement [46,47]. When the concrete specimen is subjected to rapid freeze–thaw cycles in a Na_2SO_4 solution with a mass fraction of 5%, the following reactions occur:

$$Na_2SO_4 + Ca(OH)_2 + 2H_2O \rightarrow CaSO_4 \cdot 2H_2O + NaOH \quad (1)$$

The generated $CaSO_4 \cdot 2H_2O$ (gypsum) has small grains, large dispersion, and high activity, and the reaction rate with C_3A is accelerated so that AF_t (ettringite) is rapidly generated, which greatly accelerates the hardening rate. Moreover, after the consumption of $Ca(OH)_2$, the hydration of C_3S is promoted, the hydration products are increased, and the compactness of cement stone is improved. At the same time, the presence of limestone powder causes the excess aluminum phase to react with calcium carbonate rather than with AF_t (ettringite):

$$\text{No reaction: } C_3A + AF_t \rightarrow AF_m \text{ (monosulfoaluminate)} \quad (2)$$

$$\text{Reaction: } C_3A + CaCO_3 \rightarrow M_c/H_c \text{ (single carbon/half carbon calcium aluminate)} \quad (3)$$

Therefore, the addition of limestone powder can inhibit the formation of AF_m (monosulfoaluminate) and stabilize the early formed AF_t (ettringite). The molar volume of AF_t is larger than that of AF_m, and the solid volume of hydration products increases, which reduces the porosity of the specimen. Moreover, calcium carbonate is harder and larger than AF_m, which can reduce the porosity of the specimen, reduce the pore size of the test piece, and improve the strength of the test piece, thereby improving the salt frost resistance of the CLP concrete (F and E specimens).

5. Model of Freeze–Thaw Damage

According to the theory of damage mechanics, an internal state variable "D_n" needs to be defined. It is used to describe the development of and change in material damage state and its effect on the mechanical properties of materials. It is defined as a damage variable [50]. In this section, based on the change in relative dynamic elastic modulus, the corresponding macroscopic damage evolution equation of CLP concrete is established as follows [25,51]:

$$D_n = 1 - \frac{E_n}{E_0} = 1 - P_n \quad (4)$$

where D_n is the damage variable of concrete after n freeze–thaw cycles under different freeze–thaw cycle conditions; P_n is the relative dynamic modulus of elasticity after n freeze–thaw cycles.

According to the test results, the freeze–thaw damage variables are calculated, and the results are shown in Table 4.

Table 4. The damage variable values of the concrete specimens under different freeze–thaw cycle conditions.

Number	Limestone Powder Mixing Amount (%)	Fly Ash Mixing Amount (%)	Slag Mixing Amount (%)	Freeze–Thaw Conditions	D_n (%) at Different Numbers of Freeze–Thaw Cycles				
					0 Times	25 Times	50 Times	75 Times	100 Times
A-DZ-HX	0	0	0	Water freezing cycle	0	−2.46	8.24	14.57	23.89
B-DZ-HX	10	0	0		0	5.21	13.12	18.30	27.12
C-DZ-HX	20	0	0		0	5.88	24.8	34.51	55.41
D-DZ-HX	20	30	0		0	9.13	13.87	23.62	34.27
E-DZ-HX	20	0	30		0	3.68	5.73	11.17	18.91
F-DZ-HX	20	15	15		0	3.64	5.83	13.71	21.89
A-DZ-YX	0	0	0	Salt freezing cycle	0	5.00	16.37	37.05	72.43
B-DZ-YX	10	0	0		0	1.29	18.49	33.60	/
C-DZ-YX	20	0	0		0	2.46	64.94	/	/
D-DZ-YX	20	30	0		0	3.53	62.56	/	/
E-DZ-YX	20	0	30		0	2.95	4.67	5.90	6.92
F-DZ-YX	20	15	15		0	5.93	7.04	7.72	7.04

In physics, the problem of the flat throwing of objects can be considered as the damage of gravity acceleration to height. If there is no influence of gravity acceleration, the object will be thrown to infinity. The damage reflected in the mathematical formula is the gravity acceleration g; so, the gravity acceleration can also be called the height damage acceleration of the object, in essence. Combined with the theory of damage mechanics and the principle of physics, the freeze–thaw cycles of concrete can be understood as e_g causing the relative dynamic elastic modulus damage of concrete, resulting in the nonlinear reduction in P_n [51]. The freeze–thaw damage model of CLP concrete is established as follows:

$$D_n = \frac{1}{2} e_g n^2 \tag{5}$$

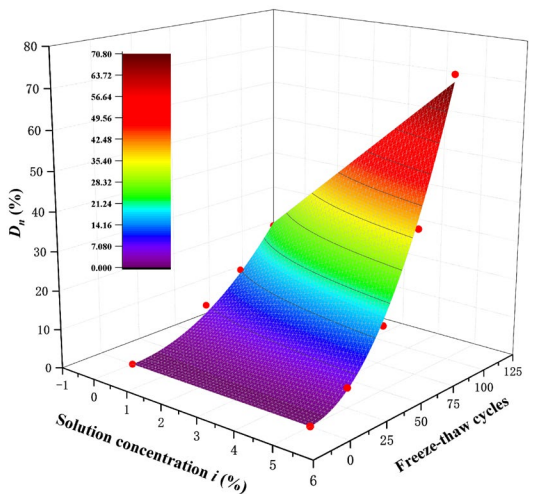
where e_g is the acceleration of the relative dynamic elastic modulus of concrete; n is the number of freeze–thaw cycles.

The relative dynamic elastic modulus of CLP concrete is greatly affected by different freeze–thaw cycle conditions (water freezing or salt freezing), resulting in great differences in its frost resistance. The concentration parameter i (0%, 5% Na_2SO_4 solution) of the freeze–thaw soaking solution is introduced here [25]. Considering different freeze–thaw cycle conditions, Origin 2022 software was used to fit the damage variable data of A, E, and F specimens under water freezing and salt freezing cycle conditions, and the freeze–thaw damage model of CLP concrete with a soaking solution concentration factor was obtained, as shown in Table 5 and Figure 10.

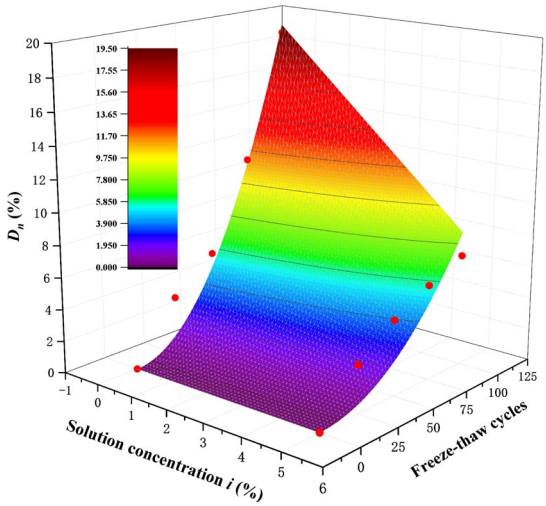
Table 5. Freeze–thaw damage model for concrete under different freeze–thaw cycles.

Specimen	Freeze–Thaw Damage Models	Correlation Coefficient R^2
A	$D_n = 1/2 \times \left(4.92 \times 10^{-3} + 1.84 \times 10^{-3} \times i\right) \times n^2$	0.9919
E	$D_n = 1/2 \times \left(3.88 \times 10^{-3} + 4.42 \times 10^{-3} \times i\right) \times n^2$	0.9076
F	$D_n = 1/2 \times \left(4.53 \times 10^{-3} + 5.14 \times 10^{-3} \times i\right) \times n^2$	0.8194

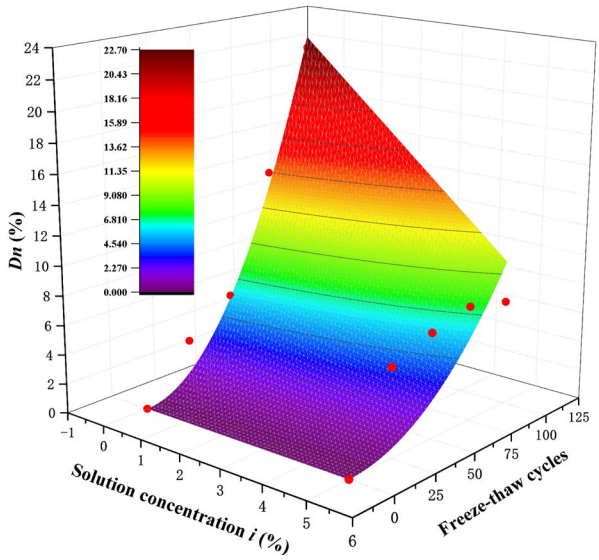
It can be seen from Table 5 and Figure 10 that the model fits the damage variable value data of A, E, and F specimens under the conditions of water freezing and salt freezing cycles, and the fitting effect is better. However, with the increase in mineral admixtures, the fitting effect of the model gradually decreases, indicating that mineral admixtures have a high impact on the frost resistance of concrete, and the impact of slag is greater than that of fly ash and limestone powder.



(**a**) Specimen A



(**b**) Specimen E



(**c**) Specimen F

Figure 10. Concrete freeze–thaw damage model in dependence of solution concentration i (%), freeze–thaw cycles, and D_n (%).

6. Conclusions

The variation rule and degradation mechanism of frost resistance of different concrete mixtures were examined from both macro and micro perspectives through the experimental investigation of CLP concrete under sulfate freeze–thaw coupling tests. The following conclusions can be drawn.

(1) Limestone powder has a filling effect, but the activity is low. When the content is between 10~20%, the chemical response is higher than the physical response. The pozzolanic effects of fly ash and slag increase the secondary hydration products, optimize the pore structure, and improve the compactness. The "superposition effect" of limestone powder, fly ash, and slag can optimize the frost resistance of CLP concrete.

(2) In the case of the fixed total content, fly ash replaces slag in equal proportion. At the physical level, the fineness of fly ash is less than that of slag, which will make the internal structure of CLP concrete loose and reduce the compactness. At the chemical level, the activity of fly ash is lower than that of slag, thereby reducing the hydration products in CLP concrete and increasing the porosity. Therefore, the frost resistances of the CLP concrete follow the indicated order: $L_{20}F_0S_{30} > L_{20}F_{15}S_{15} > L_{20}F_{30}S_0$.

(3) The coupling effect of freeze–thaw damage and sulfate attack makes the damage of salt freezing cycles to the frost resistance of CLP concrete greater than that under water freezing cycles. However, the activation of sulfate can enhance the activity effect of slag, so that the effect of slag on improving the frost resistance of concrete under salt freezing cycles is better than that of water freezing cycles.

(4) Based on the theory of damage mechanics, the freeze–thaw damage model of CLP concrete was established. Considering different freeze–thaw conditions, the damage variable values of $L_0F_0S_0$, $L_{20}F_0S_{30}$, and $L_{20}F_{15}S_{15}$ specimens under freeze–thaw cycles are fitted, and the fitting effect is better. However, mineral admixtures have a great influence on the frost resistance of concrete. With the increase in mineral admixtures, the applicability of this presented model might need more research effort.

Author Contributions: M.Z.: Conceptualization, methodology, project administration, investigation, formal analysis, and writing—original draft. H.L.: Writing—review and editing, supervision, and funding acquisition. S.Z.: Resources and data curation. Y.W.: Resources and data curation. X.Z.: Writing—review and editing, and resources. Q.Y.: Data curation. All authors have read and agreed to the published version of the manuscript.

Funding: The Graduate Innovation Program of China University of Mining and Technology (Grant No. 2022WLKXJ054) and the Research Funds for JiangSu Collaborative Innovation Centre for Building Energy Saving and Construction Technology (Grant Nos. SJXTZD2102 and SJXTBS2128).

Data Availability Statement: On reasonable request, the corresponding author will provide all or some of the data, models, or algorithms that support the study's findings.

Conflicts of Interest: The authors declare no conflict of interest.

References

1. Golaszewski, J.; Golaszewska, M.; Cygan, G. Performance of ordinary and self-compacting concrete with limestone after freeze-thaw cycles. *Buildings* **2022**, *12*, 2003. [CrossRef]
2. Junfang, H.U.O.; Zhang, S.; Jian, W.E.I.; Qi, C.U.I.; Hua, P.A.N. Experimental study on impermeability of concrete mixed with limestone powder. In Proceedings of the International Conference on Architectural Engineering and Civil Engineering (AECE) 2016, Singapore, 25–26 April 2016; pp. 236–239.
3. Wang, S.; Llamazos, E.; Baxter, L.; Fonseca, F. Durability of biomass fly ash concrete: Freezing and thawing and rapid chloride permeability tests. *Fuel* **2008**, *87*, 359–364. [CrossRef]
4. Chen, T. Study on full-slag concrete feasibility. In Proceedings of the 2nd International Conference on Advanced Engineering Materials and Technology (AEMT), Zhuhai, China, 6–8 July 2012; pp. 1682–1685.
5. Wu, Y.; Tang, P.; Lv, H.; Wei, W.; Zhou, S.; Liu, K. Degradation of the bond performance between composite limestone powder concrete and steel bars under a sulfate freeze-thaw environment. *Constr. Build. Mater.* **2023**, *369*, 130515. [CrossRef]
6. Dvorkin, L. Design estimation of concrete frost resistance. *Constr. Build. Mater.* **2019**, *211*, 779–784. [CrossRef]
7. Piekarczyk, A.; Lazniewska-Piekarczyk, B. Impact of self-compacting concrete admixtures on frost resistance and compressive strength-commensurability of frost resistance criteria. *Materials* **2021**, *14*, 2922. [CrossRef]
8. Yao, Y.; Liu, C.; Liu, H.; Zhang, W.; Hu, T. Deterioration mechanism understanding of recycled powder concrete under coupled sulfate attack and freeze-thaw cycles. *Constr. Build. Mater.* **2023**, *388*, 131718. [CrossRef]
9. Zeng, H.; Li, Y.; Zhang, J.; Chong, P.; Zhang, K. Effect of limestone powder and fly ash on the pH evolution coefficient of concrete in a sulfate- freeze-thaw environment. *J. Mater. Res. Technol.* **2022**, *16*, 1889–1903. [CrossRef]
10. Wang, D.; Shi, C.; Farzadnia, N.; Shi, Z.; Jia, H.; Ou, Z. A review on use of limestone powder in cement-based materials: Mechanism, hydration and microstructures. *Constr. Build. Mater.* **2018**, *181*, 659–672. [CrossRef]
11. Matschei, T.; Lothenbach, B.; Glasser, F.P.P. The role of calcium carbonate in cement hydration. *Cem. Concr. Res.* **2007**, *37*, 551–558. [CrossRef]
12. Mikhlif, A.-G.H.; Al-Jumaily, I.A.; Al-Numan, B.S. Mechanical properties of sustainable concrete using local limestone powder as partial replacement of cement. In Proceedings of the 12th International Conference on the Developments in eSystems Engineering (DeSE), Kazan, Russia, 7–10 October 2019; pp. 105–108.
13. Adu-Amankwah, S.; Zajac, M.; Stabler, C.; Lothenbach, B.; Black, L. Influence of limestone on the hydration of ternary slag cements. *Cem. Concr. Res.* **2017**, *100*, 96–109. [CrossRef]
14. Martin, L.H.; Winnefeld, F.; Müller, C.J.; Lothenbach, B. Contribution of limestone to the hydration of calcium sulfoaluminate cement. *Cem. Concr. Compos.* **2015**, *62*, 204–211. [CrossRef]
15. Zhang, S.; Chen, B.; Tian, B.; Lu, X.; Xiong, B. Effect of fly ash content on the microstructure and strength of concrete under freeze-thaw condition. *Buildings* **2022**, *12*, 2113. [CrossRef]

16. Panesar, D.K.; Zhang, R. Performance comparison of cement replacing materials in concrete: Limestone fillers and supplementary cementing materials—A review. *Constr. Build. Mater.* **2020**, *251*, 118866. [CrossRef]
17. Huang, Z.; Sookree, E.W.; Mohamoud, A.H.; Wang, Z. Influence of limestone powder and fly ash on the freezing and thawing resistance of roller-compacted concrete. *KSCE J. Civ. Eng.* **2021**, *25*, 2501–2507. [CrossRef]
18. Rathod, R.S.B.; Sahoo, P.; Gupta, S. Effect of microcrystalline cellulose on rheology, hydration kinetics and early-age properties of Portland cement-based and alkali-activated slag-fly ash blend. *J. Build. Eng.* **2023**, *76*, 107218. [CrossRef]
19. Irassar, E.F. Sulfate attack on cementitious materials containing limestone filler—A review. *Cem. Concr. Res.* **2009**, *39*, 241–254. [CrossRef]
20. Sun, J.; Chen, Z. Influences of limestone powder on the resistance of concretes to the chloride ion penetration and sulfate attack. *Powder Technol.* **2018**, *338*, 725–733. [CrossRef]
21. Li, X.-Y.; Chen, W.-Y.; Chen, W.-M. Multi-powder dam concrete with high performance and low adiabatic temperature rise. *Trans. Nonferrous Met. Soc. China* **2009**, *19*, S727–S733. [CrossRef]
22. Tremiño, R.M.; Real-Herraiz, T.; Letelier, V.; Ortega, J.M. Microstructure and mechanical properties of ternary mortars with brick powder, glass powder, slag, fly ash, and limestone. *Int. J. Appl. Ceram. Technol.* **2022**, *19*, 2135–2147. [CrossRef]
23. Donza, H.; Cabrera, O.; Irassar, E.F. High-strength concrete with different fine aggregate. *Cem. Concr. Res.* **2002**, *32*, 1755–1761. [CrossRef]
24. Wang, R.; Zhang, Q.; Li, Y. Deterioration of concrete under the coupling effects of freeze-thaw cycles and other actions: A review. *Constr. Build. Mater.* **2022**, *319*, 126045. [CrossRef]
25. Xiao, Q.H.; Li, Q.; Cao, Z.Y.; Tian, W.Y. The deterioration law of recycled concrete under the combined effects of freeze-thaw and sulfate attack. *Constr. Build. Mater.* **2019**, *200*, 344–355. [CrossRef]
26. Tsivilis, S.; Batis, G.; Chaniotakis, E.; Grigoriadis, G.; Theodossis, D. Properties and behavior of limestone cement concrete and mortar. *Cem. Concr. Res.* **2000**, *30*, 1679–1683. [CrossRef]
27. Adu-Amankwah, S.; Zajac, M.; Skoček, J.; Němeček, J.; Haha, M.B.; Black, L. Combined influence of carbonation and leaching on freeze-thaw resistance of limestone ternary cement concrete. *Constr. Build. Mater.* **2021**, *307*, 125087. [CrossRef]
28. Tikkanen, J.; Cwirzen, A.; Penttala, V. Freeze-thaw resistance of normal strength powder concretes. *Mag. Concr. Res.* **2015**, *67*, 71–81. [CrossRef]
29. *JGJ 55-2011*; Design of Ordinary Concrete Proportions. China State Construction, Engineering and Construction Industry Press: Beijing, China, 2011.
30. Wang, X.-Y.; Luan, Y. Modeling of hydration, strength development, and optimum combinations of cement-slag-limestone ternary concrete. *Int. J. Concr. Struct. Mater.* **2018**, *12*, 1–13. [CrossRef]
31. Zhou, J.; Qian, S.; Sierra Beltran, M.G.; Ye, G.; van Breugel, K.; Li, V.C. Development of engineered cementitious composites with limestone powder and blast furnace slag. *Mater. Struct.* **2010**, *43*, 803–814. [CrossRef]
32. *GB/T 50082-2009*; Standard for Long-Term Performance and Durability Test Methods for Ordinary Concrete. China State Construction, Engineering and Construction Industry Press: Beijing, China, 2009.
33. Li, W.; Liu, H.; Zhu, B.; Lyu, X.; Gao, X.; Liang, C. Mechanical properties and freeze-thaw durability of basalt fiber reactive powder concrete. *Appl. Sci.* **2020**, *10*, 5682. [CrossRef]
34. Cheng, H.; Liu, T.; Zou, D.; Zhou, A. Compressive strength assessment of sulfate-attacked concrete by using sulfate ions distributions. *Constr. Build. Mater.* **2021**, *293*, 123550. [CrossRef]
35. *GB/T 50081-2019*; Standard for Test Methods of Physical and Mechanical Properties of Concrete. China Stat Construction, Engineering and Construction Industry Press: Beijing, China, 2019.
36. Chen, X.; Chen, C.; Liu, Z.; Lu, J.; Fan, X. Compressive behavior of concrete under high strain rates after freeze-thaw cycles. *Comput. Concr.* **2018**, *21*, 209–217.
37. Zhang, W.; Pi, Y.; Kong, W.; Zhang, Y.; Wu, P.; Zeng, W.; Yang, F. Influence of damage degree on the degradation of concrete under freezing-thawing cycles. *Constr. Build. Mater.* **2020**, *260*, 119903. [CrossRef]
38. Wang, Y.; Liu, Z.; Fu, K.; Li, Q.; Wang, Y. Experimental studies on the chloride ion permeability of concrete considering the effect of freeze-thaw damage. *Constr. Build. Mater.* **2020**, *236*, 11755. [CrossRef]
39. Yao, X.; Zhang, M.; Guan, J.; Li, L.; Bai, W.; Liu, Z. Research on the corrosion damage mechanism of concrete in two freeze-thaw environments. *Adv. Civ. Eng.* **2020**, *2020*, 1–11. [CrossRef]
40. Liu, H.; Huang, Q.; Zhao, L. Deterioration of concrete containing limestone powder exposed to sulfate attack at ambient temperature. *Mater. Express* **2021**, *11*, 724–731. [CrossRef]
41. Wang, Q.; Yang, J.; Chen, H. Long-term properties of concrete containing limestone powder. *Mater. Struct.* **2017**, *50*, 1–13. [CrossRef]
42. Wang, D.; Shi, C.; Farzadnia, N.; Shi, Z.; Jia, H. A review on effects of limestone powder on the properties of concrete. *Constr. Build. Mater.* **2018**, *192*, 153–166. [CrossRef]
43. Sun, C.; Li, W.; Hou, B. Study on frost-salt resistance of fly ash concrete. *Adv. Mater. Res.* **2012**, *598*, 432–437. [CrossRef]
44. Shpak, A.; Gong, F.; Jacobsen, S. Frost durability of high-volume fly ash concrete: Relation liquid transport-damage. *Cem. Concr. Res.* **2023**, *163*, 107017. [CrossRef]
45. Xu, O.; Han, S.; Liu, Y.; Li, C. Experimental investigation surface abrasion resistance and surface frost resistance of concrete pavement incorporating fly ash and slag. *Int. J. Pavement Eng.* **2021**, *22*, 1858–1866. [CrossRef]

46. Alyousef, R.; Abbass, W.; Aslam, F.; Gillani, S.A.A. Characterization of high-performance concrete using limestone powder and supplementary fillers in binary and ternary blends under different curing regimes. *Case Stud. Constr. Mater.* **2023**, *18*, e02058. [CrossRef]
47. Wang, C.; Jin, Z.; Liu, G.; Dong, W.; Pang, B.; Ding, X. Mechanisms of chloride transport in low carbon marine concrete: An alkali-activated slag system with high limestone powder. *J. Build. Eng.* **2023**, *72*, 106539. [CrossRef]
48. Liu, S.H.; Wang, L. Influence of limestone powder on hydration properties of complex binders. *Mater. Res. Innov.* **2014**, *18*, 186–190. [CrossRef]
49. Shen, H.; Jiang, Y.; Xia, J. The relationship between the air void system and frost-salt resistance of concrete. In Proceedings of the 5th International Conference on Advanced Design and Manufacturing Engineering (ICADME), Shenzhen, China, 19–20 September 2015; pp. 1060–1064.
50. Voyiadjis, G.Z.; Kattan, P.I. *Damage Mechanics*; CRC Press: Boca Raton, FL, USA, 2005.
51. Yu, H.; Ma, H.; Yan, K. An equation for determining freeze-thaw fatigue damage in concrete and a model for predicting the service life. *Constr. Build. Mater.* **2017**, *137*, 104–116. [CrossRef]

Disclaimer/Publisher's Note: The statements, opinions and data contained in all publications are solely those of the individual author(s) and contributor(s) and not of MDPI and/or the editor(s). MDPI and/or the editor(s) disclaim responsibility for any injury to people or property resulting from any ideas, methods, instructions or products referred to in the content.